SURFACE TREATMENTS FOR THE SERIES PRODUCTION OF ESS MEDIUM BETA CAVITIES

M. Bertucci*, A. Bosotti, A. D'Ambros, P. Michelato, L. Monaco, C. Pagani[1], R. Paparella,
D. Sertore, INFN/LASA, Segrate (MI), Italy
A. Visentin, D. Rizzetto, M. Rizzi, E. Zanon S.p.A., Schio (VI), Italy
[1]also at Università degli Studi di Milano, Milano, Italy

Abstract

The surface treatment of ESS 704.42 MHz medium beta cavities consists of a bulk BCP 200 micron removal, a 10 h 600 °C heat treatment and a final 20 micron BCP performed after tank integration. The facility currently employed for the BCP treatment, settled in Ettore Zanon S.p.A., is here presented, together with the results so far obtained on the first series cavities in terms of frequency sensitivity, removal rate and surface external temperature. The optimization of BCP treatment by a preliminary fluid-dynamical finite element model is also discussed. Some details about the visual inspection procedure and the furnace qualification are also presented.

INTRODUCTION

INFN-LASA is currently involved in the series production of 36 $\beta = 0.67$ 704.42 MHz cavities for the ESS medium beta section. ESS specifations for medium beta cavities are $E_{acc} = 16.7 MV/m$ with a $Q_0 > 5 \cdot 10^9$ [1]. Given such moderate values, Buffered Chemical Polishing has been the natural choice as bulk and final surface treatment for the series production for ESS medium beta cavities. Due to their shape and size, a careful optimization of cavity treatment parameters has been necessary. The production of 2 prototype cavities allowed to check the process quality using the infrastructure provided by Ettore Zanon S.p.A. [2] After the bulk BCP treatment, the cavity undergoes a 600 °C 10 hours heat treatment for hydrogen degassing and a final flash BCP after the tank integration. Two optical inspections, one immediately after the electron beam welding and one after the bulk BCP, are performed to check the presence of defects at equators that could limit the cavity performance. In case of presence of defects, a grinding procedure followed by a light BCP treatment allows their complete removal of the defects. If defect size is too big to be grinded, the cavity is tested without tank in order to verify its impact on cavity performances.

BULK BCP

Cavities are treated in the Ettore Zanon Spa BCP facility located in a ISO7 clean room. The employed acid mixture is $H_3PO_4 + HNO_3 + HF$ in 2:1:1 ratio. On the whole, in order to get rid of the damaged layer, 200 μm have to be removed by the bulk BCP treatment. The treatment is divided in two batches of 90 μm and 110 μm, with the cavity

turned upside-down at the end of the first treatment so to compensate the asymmetry in the removal rate [3]. A 2 kW heat exchanger costantly cools the acid in the tank, therefore keeping acid inlet temperature below 6 °C and the outlet temperature below 15 °C.

Process Experimental Analysis

The chemical reaction rate critically depends on acid temperature, and even a modest increase of temperature could locally result in a remarkable enhancement of etching rate, in its turn heating the cavity walls and increasing the Nb temperature. For this reason, the acid inlet and outlet temperature are continuously monitored during the treatment. 8 fast reading thermocouples are installed on cavity external surface, 3 on the bottom cell, 3 on the top cell, 2 on the beam tubes. In order to control the etching rate during the process, a ultrasound transducer probe is placed in contact with cavity surface and the thickness is continuously read during the process by Olympus 38DL-plus Gage with a μm resolution. A Nb sample is inserted inside the main coupler to evaluate the material removal by the difference of weight before and after the treatment and to monitor potential surface contaminations. Figure 1 shows the position of thermocouples, niobium sample and ultrasound probe during the treatment.
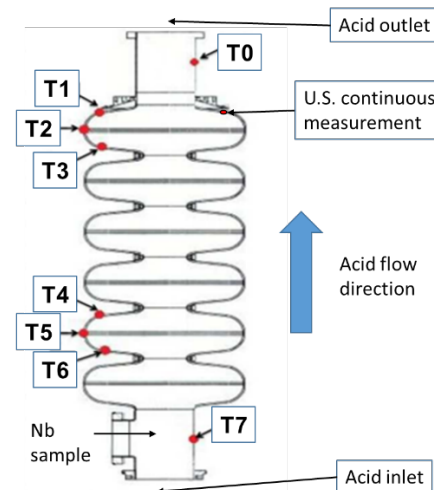

Figure 1: Position of thermocouple sensors, ultrasound probe and Nb sample during a BCP treatment.

Figure 2 shows a typical registration of thermocouple readout during a BCP process. As already noticed in [4], temperatures remains nearly constant during the treatment,

_____
* michele.bertucci@mi.infn.it

so that a constant removal is measured by the US probe during the process. However, considering different points on the same cell, temperature is higher on the face opposite to acid flow. Moreover, considering points with same orientation on different cells, temperature is considerably higher on the cell closer to the acid outlet.
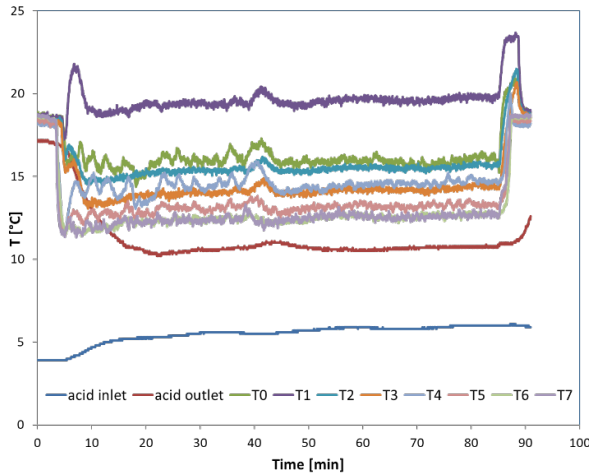

Figure 2: Temperature registration during the first bulk BCP of series cavity M001. The thermocouple labels are the same as for Fig. 1.

Such a different temperature behavior results in a not uniform removal on cavity inner surface, as confirmed by thickness measurements before and after the treatment. As an instance, Fig. 3 shows the thickness variation on several cavity points (near equator, on cell upper side, on cell lower side) for the first BCP treatment of cavity M007. Removal is higher on top cells and on the cell side opposite to acid flow, as expected by the measured temperature trend.
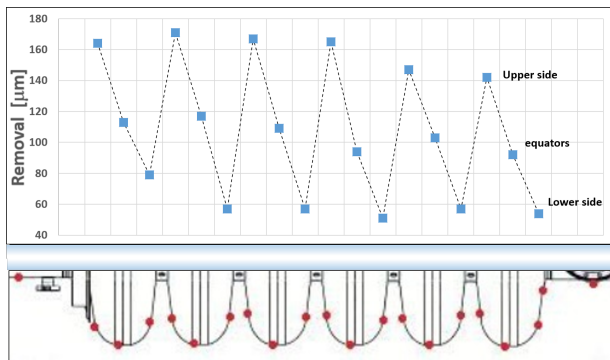

Figure 3: Thickness variation after M007 1st BCP (90 min.) measured with US probe. The acquisiton points are marked on cavity surface.

According to these experimental data, the spread in cell removal at equators is approximately 20 μm, and is considerably lower than difference in removal between opposite sides on the same cell, that reaches in this case even more than 100 μm. Hence, the cavity reversal has a double beneficial effect. Besides correcting the cell to cell removal asymmetry, it also equalizes the removal difference on opposite sides of the same cell.

BCP Fluid Simulation

The strong and unexpected asymmetry in wall temperature profile and removal rate can be due to local variations of fluid velocity and temperature. As shown in [5], etching rate at different fluid velocity can be fitted with a power law: as the velocity increases the etching rate increases. Same results have been observed with temperature changes. To better understand this behaviour, we performed a series of fluid dynamic simulations whose purpose is to reproduce the velocity field inside the cavity during a BCP treatment. Starting from this very first results, one can start to argue about more complex behaviours observed during the real processes.

The key parameter needed to define the fluid behavior inside the cavity is the Reynolds Number, $Re = \frac{\rho v D}{v}$, where ρ is the acid density, v is the acid velocity at the inlet, D is inlet diameter and v is the acid viscosity. Density and viscosity are calculated by weighing the single component values on the concentration in the mixture, considering also their temperature dependence. Inlet diameter and liquid velocity are calculated from the characteristics of the plant and from process throughput. A value $Re = 706$ is obtained, which corresponds to laminar flow. However, as stated in [6], the heat of reaction is dissipated in the BCP fluid through convective motions. Therefore, a transition from laminar to turbulent flow takes place near the cavity wall and a suitable turbulent model has to be employed.

Fluid simulations have been performed with the fluid solver Ansys Fluent. The first trial has been done with costant temperature, and therefore also BCP fluid viscosity, by assuming adiabatic walls. Simulation results highlight three different fluid-dynamical regimes:

- the fluid velocity field on cavity axis remains laminar, so that the fluid column coming out from the inlet doesn't break as would happen in turbulent flow. Instead, it slowly increases its diameter as it proceeds towards the outlet and its average velocity (of the order of $10^{-1} m/s$) slowly decreases. From now we will call *main column* this flow region.

- Once the fluid arrives at the cavity outlet, the increase in diameter of the main column leads to a subdivision of the flux: part of it flows through the outlet, while the remaining part hit the upper flange and reverses its direction. Here is the main place where the fresh mixture is mixed with the old one. A secondary motion arises: between the main column and the cavity irises there is a recirculation that affects the entire length of the cavity. This motion laps the cells whitout entering. Iris works as nozzle increasing the velocity of this recirculation. In this region the velocity is in the order of $10^{-2} m/s$. From now we will call *main recirculation* this flow region.

- Inside each cells a third different motion takes place. The velocity is in the order of $10^{-3} m/s$. From now we will call *cell recirculation* this flow region. The transition between the main recirculation and the cell recirculation takes place at the lower part of each cell.

The main column flows from the lower part of the cavity towards the upper part. The main recirculation flows counter-clockwise while the cell recirculation flows clockwise. A typical reconstruction of path lines in laminar regime is shown in Fig. 4
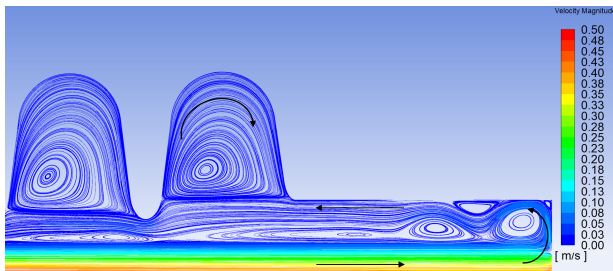

Figure 4: Path line in laminar solution. Main column, main recirculation and cell recirculation zones can be noticed.

As second step, the thermal behavior of the system is considered. A complex series of strongly exothermic chemical reactions took place at cavity surface. As first attempt, we simulate this reaction as a constant heat flux over the cavity wall. A $q = 960 \frac{W}{m^2}$ value is assumed as heat of reaction [7]. Simulation results highlight that:

- As for the velocity field, the same three different zones can be identified even for temperature. Velocity is overall higher both in the main and the cell recirculation, which also have different average temperatures. In the main column the temperature remains almost constant and equal to inlet temperature. This correspondance is probably due to the low thermal conductivity and velocity of the BCP fluid which prevents any mixing.

- At the iris, where velocity is higher, temperature is lower than any other part of the cavity surface. Here all the heat flux is extracted by the fast stream and used to heat the whole main recirculation. The same behaviour is observed inside the cell, where the temperature is lower and the velocity higher.

- The upper part of the cells is hotter than the lower part, as expected from experimental data. However the lower cells are on average hotter than the higher, in contrast with experimental data.

- Difference of temperature between inlet and outlet is evaluated as $\Delta T = 2.87K$, in agreement with experimental results.

The constant heat flux model is obviously an oversimplified picture. Since the cell recirculation is closed inside the cell while at the iris we always have a fast flow, we imposed

that the main heat exchange take place at the iris, so the heat flux is better modeled by a sinusoidal profile with maximum at irises position. Figure 5 shows the reconstructed temperature profile on cavity surface.
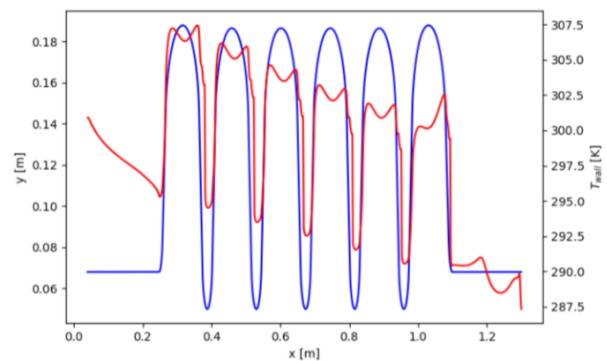

Figure 5: Cavity (blue) and temperature profile (red) assuming a sinusoidal profile for heat flux. Acid enters from left side.

Again we obtain lower cells hotter than the higher cells. This is probably due to the fact that upper cells are actually reacting with a fresher acid mixture. It is known that kinetics of reaction is also influenced by the concentration of dissolved NO_x species that are by-products of the etching reaction and may partially inhibit the reaction at the end of the recirculation, namely at lower cells. In the future the model will be extended also taking into account this effect.

Analysis of Series Production

At the present time, 18 ESS medium β cavities have been fully BCP treated at the Zanon facility. As already stated, the foreseen average removal is 200 μm. This value can be anyhow partially changed in order to adjust the overall cavity frequency variation, in the case of a cavity frequency after EBW significantly different from the nominal value. The lower limit we assumed for a safe surface removal of damaged layer is 180 μm. Conversely, the overall BCP removal can be deliberately increased without any concern. On the whole, such modifications of treatment baseline recipe has been adopted two times:

- In the case of cavity M004, a preliminary grinding has been performed in order to remove imperfections produced during EBW, followed by a longer BCP stage (340 μm), needed to get rid of grinding residuals.

- cavity M007 frequency after 1st BCP was lower than expected. In order to get as closest as possible to the goal value, the second BCP stage has been reduced to 70 μm.

Table 1 shows the average values of the characteristic treatment parameters for the standard bulk BCP process. The average surface removal is evaluated from the difference of cavity weight before and after the treatment. Excluded from this evaluation are the two previously mentioned cases.

Table 1: Average Values of Characteristic Treatment Parameters for the 2 BCP Steps

Item	1st step BCP	2nd step BCP
removal (µm)	96 ± 7	107 ± 11
frequency shift (kHz)	283 ± 22	307 ± 38
etching rate (µm min^{-1})	1.08 ± 0.06	1.05 ± 0.04
sensitivity (kHz µm^{-1})	2.98 ± 0.24	2.86 ± 0.23

Figure 6 shows the overall frequency sensitivity and the average surface removal for the two treatment steps. Relative variation is below 10% for frequency sensitivity and below 5% for etching rate. This means that the procedure so far employed grants enough reproducibility of cavity surface treatment. The marginally higher spread in frequency sensitivity is due to slight differences in the iris-equator etching ratio which cannot be directly measured by US probe due to the presence of stiffening rings in irises. No direct relationship between sensitivity variations and temperature readings during the process can be noticed. It must be however stressed that this secondary effect has no impact on cavity production.
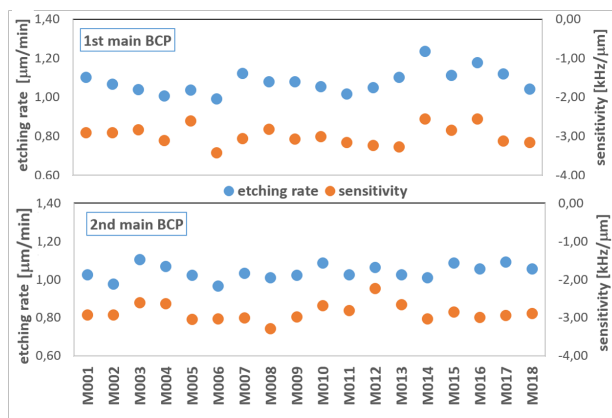

Figure 6: Measured sensitivity and removal rate for the two BCP steps of the first 18 series production cavities.

ANALYSIS OF CAVITY SURFACE

An optical inspection tool has been developed so to inspect the inner cavity surface at irises and equators. The setup employs a monochrome autofocus camera with 8 MP resolution and interchangeable M12-mount lenses, therefore adapting to different object distances. In the ESS cavity case, a 12 mm focal length lens is employed for the equator surface inspection, which corresponds to a 27° field of view on cavity equator direction and allows enough depth of field to keep the image focused on the cavity axis direction. With this configuration, the device is able to identify geometric features of 50 µm size. If necessary, this limit can be pushed down to 30 µm by mounting a 16 mm lens. The visual inspection is performed immediately after the EBW and after the bulk BCP treatment. In case a cavity needs a local de-

fect grinding, the inspection is repeated until a satisfactory surface condition is reached.

The optical inspection has been succesful in detecting surface defects in many cases. The most common issue so far encountered is the presence of local pitting after the BCP treatment. As an instance, Fig. 7 shows one defect found on cavity M008. Its characteristic size is of the order of 1 mm.
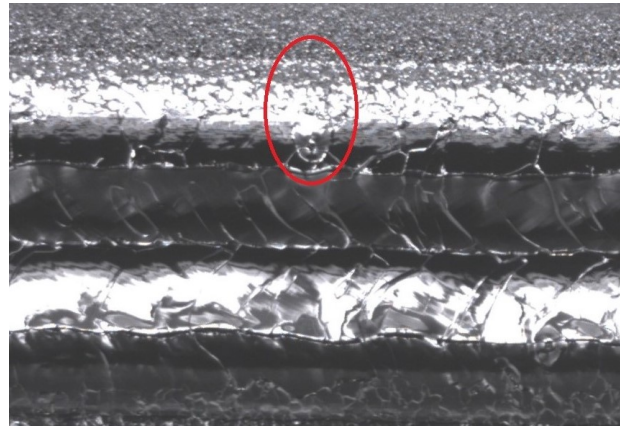

Figure 7: Optical inspection image of cavity M008 at eq.1.

As first attempt of restoring the surface, we proceeded with an intensive local grinding. But such procedure has been uneffective and the defects were still present even after several hours of grinding, meaning that such pits were too deep to be easily removed mechanically. Some replicas have been taken, in order to reconstruct the 3D profile of the defect. The replica have been then analyzed with a 3D digital microscope with a 200X magnification. The 3D reconstruction of one of the defects is shown in Fig. 8, with an evaluation of Z profile at the maximum height. The defect depth is of the order of 100 µm. This explains why the grinding procedure has not been incisive.
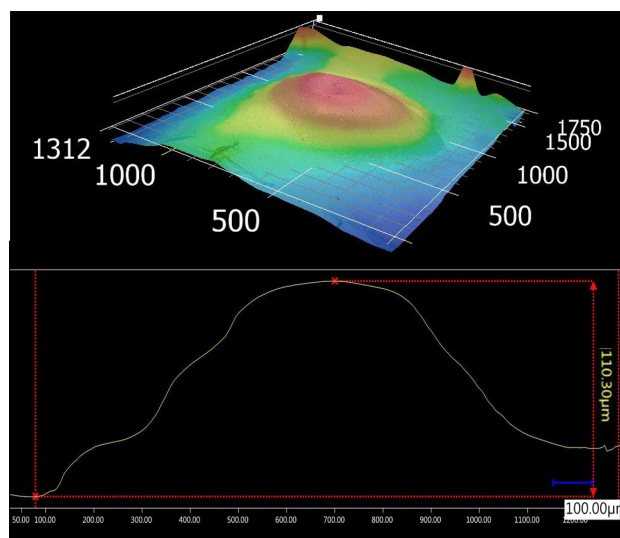

Figure 8: 3D microscope image of a defect in cavity M008.

Being aware that such defects could limit the cavity performance through a premature thermal breakdown mechanism, we decided to test, before the tank integration, two of the series which exhibited the most pronounced pitting, namely cavity M006 and M010. Indeed, both cavities quenched at a field slightly lower than the average value of series production [8], but well above the specification value of ESS medium beta cavities. In the meantime, an in-depth quality control of the production steps - from cavity assembly to EBW - has been performed. Thanks to the intensification of such control procedure, the pitting phenomenon after BCP is almost disappeared on the last series cavities.

FURNACE QUALIFICATION

After an accidental venting event occurred at high temperature, the inner surface of E. Zanon furnace underwent a sudden oxydization reaction. A long decontamination procedure has then been necessary to recover the vacuum conditions needed for the safe heat treatment of ESS medium-beta cavities, namely a pressure below $3 \cdot 10^{-5}$ mbar in the oven with a low content of hydrocarbons - as detected by RGA spectrometer - during the whole thermal cycle.

Once these conditions were met, a further qualification test has been performed by heat treating some niobium samples obtained from the sheets of ESS cavity production. Different thermal cycles (10 h at 600 °C, 2 h at 800 °C, 2 h at 1000 °C) have been checked. Adopting a conservative approach, we assumed 800 °C as qualification temperature, although the heat treatment for ESS cavity is planned at 600 °C.

As first check, RRR is measured on different samples before and after the treatment. On average, RRR decreases of 7% after the treatment. The maximum variation registered is of 13%. Such values are in line with typical variations registered in other furnaces [9], and are well within the RRR measurement reproducibilty.

After the bulk, the surface state of the samples is analyzed. Many residual gases in furnace are expected to diffuse only in the first μm of niobium, and such surface segregation is not expected to produce any significative variation in RRR. Hence, the sample surface is anayzed by SEM-EDX and the depth profile on the first 10 μm for several elements is acquired by means of GDOES (Glow Discharge Optical Emission Spectroscopy) technique. SEM-EDX analysis detected some minor and sporadic surface contaminations (max 20 μm size), which are equally present on both blank and heat treated samples. This means that no new surface impurities have been produced by the treatment. From GDOES side, the only substantial difference in depth profile were detected for:

- Hydrogen: the surface concentration decreases after heat treatment, as expected from high temperature degassing.

- Carbon: after the heat treatment, concentration increases in the first μm, following a typical diffusion profile.
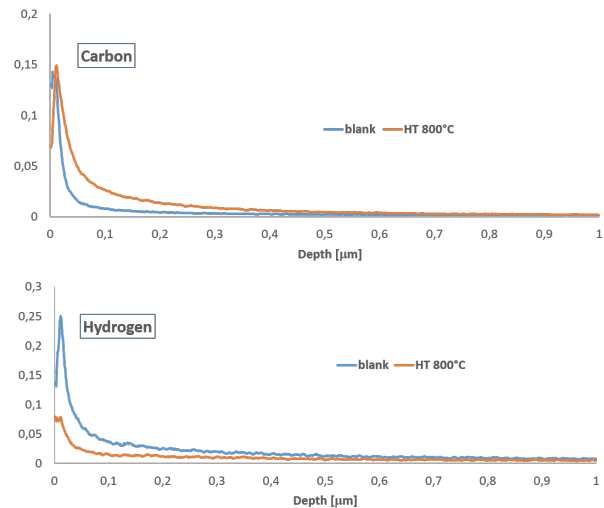

Figure 9: Depth profile by GDOES for hydrogen and carbon on the first μm. Intensity is in a.u.

Such profiles are shown in Fig. 9. Carbon diffusion length is less than 1 μm. One can therefore assume that, after the final BCP removal (20 μm), the optimal surface condition is again restored. This behavior is consistent with the increase of carbon diffusivity with temperature, but also with the RGA data acquired at 800 °C, that displayed a background of hydrocarbons slightly higher than the one at 600 °C.

Given these considerations, we consider the fornace again qualified to perform the heat treatment of ESS medium beta cavities. In the next weeks, cavity M013 will undergo the standard 600 °C heat treatment in Zanon and will be then tested without tank at the LASA vertical test facility.

CONCLUSION

The acvity of INFN-LASA on surface treatments for the series production of ESS medium-beta cavites is presented. The bulk BCP recipe has proven to provide stable and reliable results in terms of removal rate and frequency variation. The final surface quality has been remarkably improved thanks to an effort in optiimizing the quality of the production cycle. The furnace for cavity treatment underwent a qualification procedure by means of bulk and surface analysis of Nb samples. This facility is now ready for the annealing of series production cavities. On the whole, the series production is at the turning point, with 18 cavities already treated and as many to be treated in the next weeks.

REFERENCES

[1] P. Michelato *et al.*, "Status of the ESS Medium Beta Cavities at INFN - LASA", in *Proc. 10th Int. Particle Accelerator Conf. (IPAC'19)*, Melbourne, Australia, May 2019, pp. 2211-2214. doi:10.18429/JACoW-IPAC2019-TUPTS119

[2] L. Monaco *et al.*, "Fabrication and Treatment of the ESS Medium Beta Prototype Cavities", in *Proc. 8th Int. Particle Accelerator Conf. (IPAC'17)*, Copenhagen,

Denmark, May 2017, pp. 1003–1006. `doi:10.18429/JACoW-IPAC2017-MOPVA060`

[3] E. Cenni *et al.*, "Vertical Test Results on ESS Medium and High Beta Elliptical Cavity Prototypes Equipped with Helium Tank", in *Proc. 8th Int. Particle Accelerator Conf. (IPAC'17)*, Copenhagen, Denmark, May 2017, pp. 948–950. `doi:10.18429/JACoW-IPAC2017-MOPVA041`

[4] M. Bertucci *et al.*, "LASA Activities on Surface Treatment of Low-beta Elliptical Cavities", in *Proc. 10th Int. Particle Accelerator Conf. (IPAC'19)*, Melbourne, Australia, May 2019, pp. 2207-2210. `doi:10.18429/JACoW-IPAC2019-TUPTS118`

[5] F. Eozénou *et al.*, "Investigation of BCP Parameters for Mastery of SRF Cavity Treatment", in *Proc. 18th Int. Conf. RF Superconductivity (SRF'17)*, Lanzhou, China, Jul. 2017, pp. 558–562. `doi:10.18429/JACoW-SRF2017-TUPB072`

[6] T. J. Jones *et al.*, "Determining BCP Etch Rate and Uniformity in High Luminosity LHC Crab Cavities", in *Proc. 18th Int. Conf. RF Superconductivity (SRF'17)*, Lanzhou, China, Jul. 2017, pp. 635–639. `doi:10.18429/JACoW-SRF2017-TUPB100`

[7] I. M. Malloch, L. J. Dubbs, K. Elliott, R. Oweiss, and L. Popielarski, "Niobium Reaction Kinetics: An Investigation into the Reactions Between Buffered Chemical Polish and Niobium and the Impact on SRF Cavity Etching", in *Proc. 3rd Int. Particle Accelerator Conf. (IPAC'12)*, New Orleans, LA, USA, May 2012, paper WEPPC066, pp. 2360–2362.

[8] A. Bosotti *et al.*, "Vertical Test of ESS Medium Beta Cavities", in *Proc. 10th Int. Particle Accelerator Conf. (IPAC'19)*, Melbourne, Australia, May 2019, pp. 2852-2855. `doi:10.18429/JACoW-IPAC2019-WEPRB023`

[9] P. Bauer *et al.*, "Recent RRR measurements on Niobium for Superconducting RF Cavities at Fermilab", in *Proc. 12th Int. Conf. RF Superconductivity (SRF'05)*, Ithaca, NY, USA, Jul. 2005, paper TUP47, pp. 352–354.